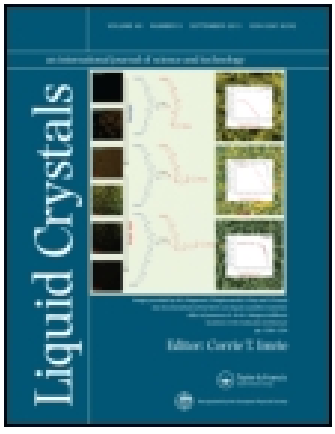

Liquid Crystals
Publication details, including instructions for authors and subscription information:
http://www.tandfonline.com/loi/tlct20

Optical hyperbolic metamaterials based on nanoparticles doped liquid crystals

Dan Jia[ab], Chengliang Yang[a], Xiaoping Li[ab], Zenghui Peng[a], Yonggang Liu[a], Zhaoliang Cao[a], Quanquan Mu[a], Lifa Hu[a], Dayu Li[a], Lishuang Yao[a], Xinghai Lu[a], Xiangjun Xiang[ab], Hongsheng Zhang[c] & Li Xuan[a]

[a] State Key Laboratory of Applied Optics, Changchun Institute of Optics, Fine Mechanics and Physics, Chinese Academy of Sciences, Changchun, P.R. China

[b] Graduate School of the Chinese Academy of Sciences, Beijing, P.R. China

[c] Grating Technology Laboratory, Changchun Institute of Optics, Fine Mechanics and Physics, Chinese Academy of Sciences, Changchun, P.R. China

Published online: 14 Nov 2013.

To cite this article: Dan Jia, Chengliang Yang, Xiaoping Li, Zenghui Peng, Yonggang Liu, Zhaoliang Cao, Quanquan Mu, Lifa Hu, Dayu Li, Lishuang Yao, Xinghai Lu, Xiangjun Xiang, Hongsheng Zhang & Li Xuan (2014) Optical hyperbolic metamaterials based on nanoparticles doped liquid crystals, Liquid Crystals, 41:2, 207-213, DOI: 10.1080/02678292.2013.847126

To link to this article: http://dx.doi.org/10.1080/02678292.2013.847126

Liquid Crystals, 2014
Vol. 41, No. 2, 207–213, http://dx.doi.org/10.1080/02678292.2013.847126

Optical hyperbolic metamaterials based on nanoparticles doped liquid crystals

Dan Jia[a,b], Chengliang Yang[a]*, Xiaoping Li[a,b], Zenghui Peng[a], Yonggang Liu[a], Zhaoliang Cao[a], Quanquan Mu[a], Lifa Hu[a], Dayu Li[a], Lishuang Yao[a], Xinghai Lu[a], Xiangjun Xiang[a,b], Hongsheng Zhang[c] and Li Xuan[a]

[a]*State Key Laboratory of Applied Optics, Changchun Institute of Optics, Fine Mechanics and Physics, Chinese Academy of Sciences, Changchun, P.R. China;* [b]*Graduate School of the Chinese Academy of Sciences, Beijing, P.R. China;* [c]*Grating Technology Laboratory, Changchun Institute of Optics, Fine Mechanics and Physics, Chinese Academy of Sciences, Changchun, P.R. China*

(*Received 5 June 2013; accepted 17 September 2013*)

Self-aligned liquid crystals containing randomly dispersed nanoparticles are proposed to realise hyperbolic metamaterials at visible spectrum. Opposite signs for anisotropic permittivity tensors originated from the scattering of metallic nanoparticles in liquid crystals are achieved. Tunable effective wavelength properties are also demonstrated by choosing dielectric-metal core-shell nanoparticles.

Keywords: metamaterials; resonance; liquid crystals; nanoparticle

1. Introduction

Hyperbolic metamaterials (HMs) which are regarded as promising artificial engineered structures for realising negative refraction have been focused on by many researchers [1–7]. The signs of dielectric tensors along different principal axis are opposite. Unlike negative index materials that require both negative permittivity and permeability, there is no requirement for negative permeability in HMs, and therefore, it is easier to realise broad band all-angle negative refraction. Although one cannot use a single slab of HMs as a super lens like negative index metamaterials, HMs have the ability to realise hyperlens [8–10] due to the fact that evanescent waves can be converted to propagating waves in HMs. Besides, there are many exotic potential applications, such as subwavelength imaging, nanoscale waveguiding, biosensing and nonlinear switching [11].

So far, researches mainly focus on two kinds of HMs structures consisting of metallic nanowire arrays embedding in dielectric matrix and metal-dielectric alternating multilayer films. Experimental works have been realised in the structure Al_2O_3/silver in optical frequency range [2,12,13] and $In_{0.53}Ga_{0.47}As$/$Al_{0.48}In_{0.52}As$ semiconductor film in mid-infrared range [14]. Recently, low loss HMs based on Al/ZnO film at near-infrared wavelength is also demonstrated experimentally [7]. However, all such HMs mentioned above need very complex and expensive fabrication craft. Hence, there is a growing interest in exploiting easily prepared new structured HMs with additional novel properties, such as tunable and flexible.

Mie resonances of dielectric and metal spheres have been investigated extensively in metamaterials [15–20]. Dielectric with high permittivity either single constituent spheres or core-shell spheres are used to obtain negative permeability and negative refractive index. In this paper, we propose an alternative approach to design HMs based on Mie resonance of metallic nanoparticle in visible frequency range. The structure is composed of self-aligned liquid crystals (LCs) and randomly dispersed metallic nanoparticles. In long wavelength limit conditions, the effective permittivities of metallic nanoparticle doped LCs can be described as anisotropic dielectric tensors. Due to opposite signs of dielectric tensors along different axis of LCs molecule, hyperbolic dispersion relations are achieved near 500 nm wavelength range. HMs can also be extended to other wavelength range through the core-shell nanoparticles doping. Unlike HMs based on medium mixing rules, HMs we proposed in this paper is based on Mie theory and Lorentz–Lorenz formula.

2. Effective medium theory

When the incident plane wave with wavelength λ goes to subwavelength metallic sphere with radius R, in long wavelength limit condition $\lambda >> R$, the single metallic sphere is equivalent to an electric dipole. The effective electric polarisability α_e is derived from [21]

$$\alpha_e = 6\pi i a_1 / k_{\mathrm{LC}}^3 \tag{1}$$

where k_{LC} is wave number in LCs. The Mie scattering coefficient is given as follows:

*Corresponding author. Email: ycldahai@gmail.com

$$a_m = \frac{n\psi_m(nx)\psi'_m(x) - \psi_m(x)\psi'_m(nx)}{n\psi_m(nx)\xi'_m(x) - \xi_m(x)\psi'_m(nx)} \tag{2}$$

where ψ_m and ξ_m are the Riccati–Bessel functions and m is the index term. The primes indicate differentiation with respect to the argument. The relative refractive index n is the ratio of index of metal sphere to the LCs. The size parameter x is $k_{\mathrm{LC}}R$.

The corresponding efficiency factor Q_{sca} of scattering cross section is as follows:

$$Q_{\mathrm{sca}} = \frac{2}{x^2}\sum_{m=1}^{\infty}(2m+1)|a_m|^2 \tag{3}$$

In the long wavelength condition, the first order term dominates the scattering. So, high order terms can be ignored in the calculations. The efficiency factor is simplified as follows:

$$Q_{\mathrm{sca}} \approx \frac{6}{x^2}|a_1|^2 \tag{4}$$

Using Lorentz–Lorenz formula, the effective permittivity tensors of metallic nanoparticle doped LCs can be described as follows:

$$\varepsilon'_{\mathrm{LC}} = \varepsilon_{\mathrm{LC}}\frac{3+2N\alpha_e}{3-N\alpha_e} \tag{5}$$

where $N = 3f/4\pi R^3$, f is the volume fraction of metallic nanoparticles. $\varepsilon_{\mathrm{LC}}$ is the permittivity of LCs. The nanoparticle incorporation does not change the anisotropic property and only changes the values of permittivity tensors.

3. Results and discussions

The alignment of LC molecule is schematically shown in Figure 1(a). The director axis is perpendicular to substrates. The permittivity tensors are described as $\varepsilon_{||}$ and $\varepsilon_{\perp}$ along and perpendicular to director axis, respectively. Large anisotropic LCs with $\varepsilon_{||} = 4$ and $\varepsilon_{\perp} = 2$ [22] were selected to perform metallic nanoparticle doping. Owing to small energy dissipation among noble metals, silver is chosen as the doped nanoparticles. For nanometer-sized metallic nanoparticles, confinement effect drastically increases the scattering rate for the surface of the particle. This confinement effect is due to the modulation of damping constant γ_0 which results from the adding the surface scattering rate $\omega_s = A\upsilon_f/R$, where υ_f is the Fermi velocity (e.g., $1.4 \times 10^8 cm/s$ for silver), R is the radius of the nanoparticle and A is a proportionality factor (0.25 for silver). So, the permittivity of nanometer-sized silver particles can be expressed as [23–26]

$$\varepsilon(\omega, R) = \varepsilon_{\mathrm{bulk}}(\omega) + \frac{f_0\omega_p^2}{\omega^2 + i\omega\Gamma_0} - \frac{f_0\omega_p^2}{\omega^2 + i\omega(\Gamma_0 + A\upsilon_F/R)} \tag{6}$$

where the bulk permittivity ε_{bulk} is given by

$$\varepsilon_{\mathrm{bulk}}(\omega) = \varepsilon_{\mathrm{free\_electron}}(\omega) + \varepsilon_{\mathrm{interband}}(\omega) = 1 - \frac{f_0\omega_p^2}{\omega(\omega + i\Gamma_0)} + \sum_{j=1}^{k}\frac{f_j\omega_p^2}{\omega_j^2 - \omega^2 - i\omega\Gamma_j} \tag{7}$$

where ω_p is the plasma frequency, f_0 and Γ_0 are the oscillator strength and damping frequency associated with interband transitions, and f_j and Γ_j are the oscillator strengths and damping frequency of the j oscillators modelling interband transitions. The values of these parameters for silver are taken from literature [26].

The incorporation of silver nanoparticles strongly affects the effective electric polarisability along different directions of LCs. When the volume fraction of silver nanoparticles is big enough, permittivity tensor along one direction of LC molecule will vary from positive to negative. In contrast, tensors along the other

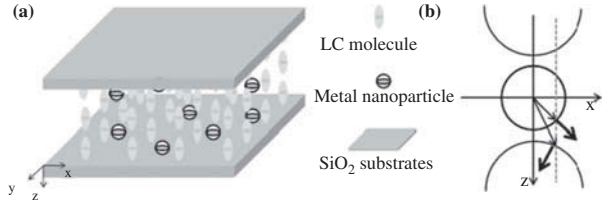

Figure 1. (colour online) (a) Schematic representation of homeotropic aligned liquid crystal molecule with randomly dispersed metallic nanoparticles. (b) The hyperbolic dispersion contour results in all-angle negative refraction in the interface between the air and HMs.

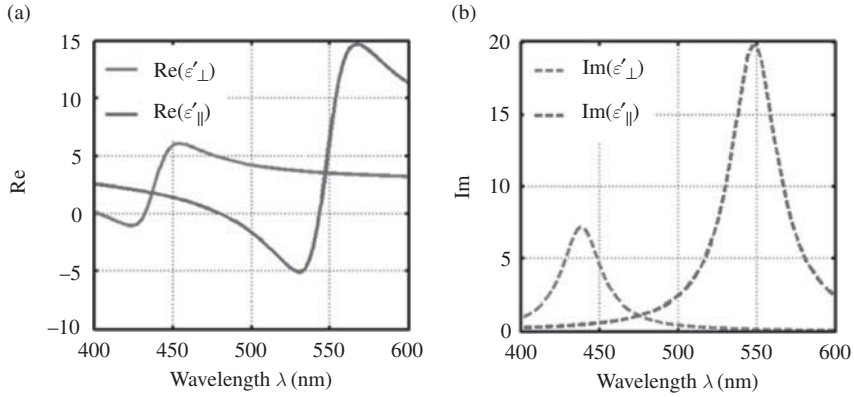

Figure 2. (colour online) (a) Real part and (b) imaginary part of effective anisotropic permittivities for liquid crystals with randomly dispersed silver nanoparticles.

directions remain positive. The appearance of negative permittivity tensor leads to hyperbolic dispersion relation as shown in Figure 1(b). The hyperbolic dispersion is given as $k_z^2/\varepsilon_\perp - k_x^2/\varepsilon_{||} = k_0^2$. When a beam with magnetic field polarised along Y direction incidents from air to such materials, all-angle negative refraction will occur at the interface.

3.1 Permittivity tensors with opposite signs

The results for real and imaginary parts of anisotropic permittivity tensors are shown in Figures 2(a) and 2(b). The radius of silver nanoparticle is $R = 10$ nm and volume fraction is $f = 0.1$. It is seen that negative $\mathrm{Re}(\varepsilon'_{||})$ appears in approximately 480–540 nm, but $\mathrm{Re}(\varepsilon'_\perp)$ remains positive. For transverse magnetic (TM) polarised light (magnetic field polarises along Y direction as shown in Figure 1(a)) in such material would obey hyperbolic dispersion relation which produces all-angle negative refraction. From Figure 2(b), there are two peaks for imaginary parts of anisotropic permittivity tensors. Between the peaks, the two imaginary parts both are small, HMs could work in this wavelength range with low energy dissipation. The imaginary part of $\varepsilon'_{||}$ increases drastically in the long wavelength side which means strong energy dispassion for this HM.

The efficiency factor Q_{sca} is plotted as a function of wavelength λ as shown in Figure 3. We can see that scattering are different along different directions. The scattering peaks locate on different wavelength positions and the scattering strength for parallel direction is stronger than perpendicular direction. Adequate metallic nanoparticles doping in LC will change the dielectric properties, as a result negative permittivity tensors appear. When a TM light propagates in the composite structure, negative refraction appears. The working wavelength for such materials depends on anisotropic permittivity of LCs host.

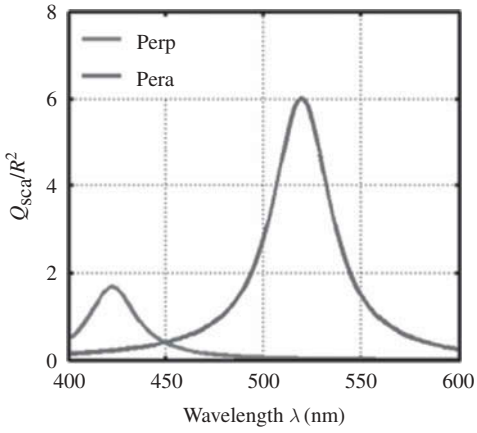

Figure 3. (colour online) Efficiency factor Q_{sca} for perpendicular (-Perp) and parallel (-Para) directions to liquid crystal alignment.

For larger anisotropic LCs, wavelength range realising negative refraction is wider.

In addition, as shown in Figure 2 there is a wavelength range near 420 nm in which $\varepsilon'_{||} > 0$ and It is because the scattering peak for perpendicular direction is just in this wavelength range, but parallel direction is not as shown in Figure 3. The analysis for this range is the same as mentioned above and the only difference is the exchange of the role for transverse electric (TE) and TM light. In other words, negative refraction can be achieved for TE polarised light in this range.

Anisotropic permittivity tensors in doped LC strongly depend on the volume fraction f of metallic nanoparticles. Although negative permittivity is obtained easily for large volume fraction, large volume fraction will cause big imaginary part and the forming of LC phase will be more difficult. In experiment, we should choose reasonable volume fraction to deal with the contradiction. In Figure 4, we plot the effective permittivity tensors as the function

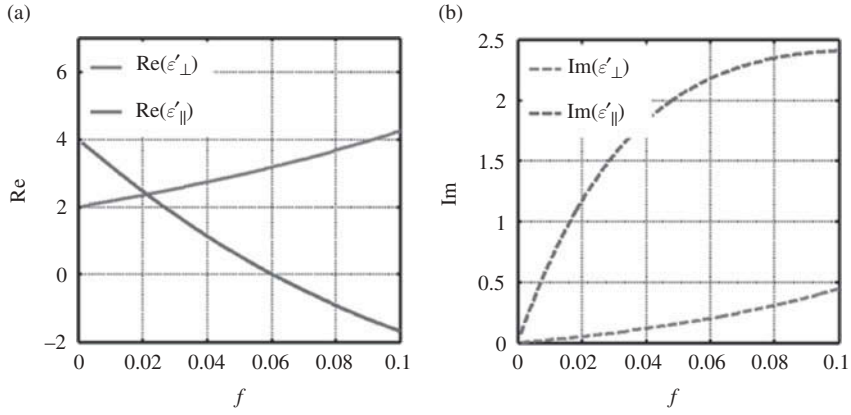

Figure 4. (colour online) (a) Real part and (b) imaginary part of effective permittivity tensor as a function of volume fraction f at 500 nm. The radius is 10 nm.

of the volume fraction f at $\lambda = 500$ nm. Real part of $\varepsilon'_{||}$ changes from positive to negative when f increases more than 0.06 and the imaginary part is approximately 2 in this fraction range. Real part of $\varepsilon'_\perp$ varies from 2 to 4 as f increasing from 0 to 0.1 and the imaginary part is smaller than 0.5 all the time. From these analyses, we can see that large volume fraction f can help us to realise negative permittivity tensor, but the imaginary part increases correspondingly which leads to much stronger energy dissipation.

3.2 *Tunable wavelength range*

Due to the limitation of scattering property of silver nanoparticles, the working wavelength for HMs is difficult to be extended to other visible range. As an approach, we can choose core-shell nanoparticles instead of the silver particle. The related Mie scattering coefficient of core-shell spherical particle is modified as follows [27]:

$$a_m = \frac{\psi_m(y)[\psi'_m(n_2y) - A_m\chi'_m(n_2y)] - n_2\psi'_m(y)[\psi_m(n_2y) - A_m\chi_m(n_2y)]}{\xi_m(y)[\psi'_m(n_2y) - A_m\chi'_m(n_2y)] - n_2\xi'_m(y)[\psi_m(n_2y) - A_m\chi_m(n_2y)]} \tag{8}$$

where $\psi_m(z) = zj_m(z)\,\xi_m(z) = zh_m^{(1)}(z)$ and $\chi_m(z) = -zy_m(z)$ are Ricatti–Bessel functions, $h_m^{(1)}(z) = j_m(z) + iy_m(z)$ is the spherical Hankel function of the first class. The coefficient A_l is

$$A_l = \frac{n_2\psi_m(n_2x)\psi'_m(n_1x) - n_1\psi'_m(n_2y)\psi_m(n_1x)}{n_2\chi_m(n_2x)\psi'_m(n_1x) - n_1\chi'_m(n_2x)\psi_m(n_1x)} \tag{9}$$

where $x = k_hR_1$ and $y = k_hR_2$. n_1 and n_2 are the ratios of the refractive indices of core and shell material to the index of LC host.

By adjusting the inner and outer radius, the working wavelength range for such materials can be tuned to other visible spectrum. For example, core-shell nanoparticles used in this paragraph are silicon oxide (SiO_2) cores and silver coatings. The permittivity of SiO_2 is assumed to be 2. It is shown in Figure 5(a)

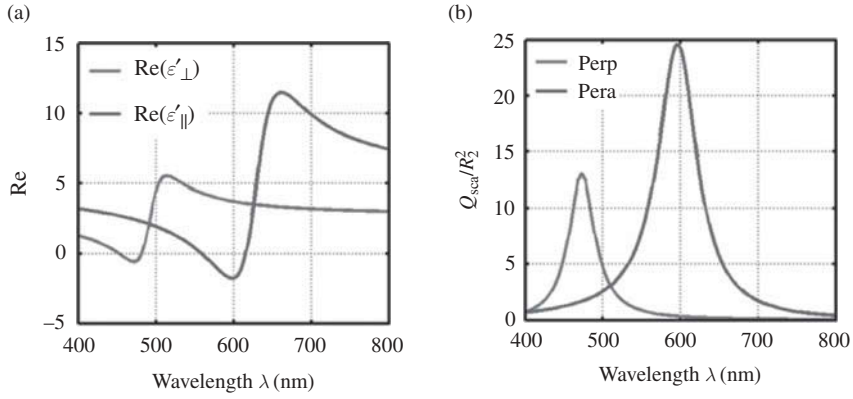

Figure 5. (colour online) (a) Calculated real parts of effective permittivity tensors for doped liquid crystals. Volume fraction is 0.1. (b) The scattering sections for SiO_2/Ag core-shell nanoparticles with $R_1 = 10$ nm and $R_2 = 20$ nm.

that wavelength range achieving negative $\varepsilon'_{||}$ is approximately 560–610 nm. As shown in Figure 5(b), the peaks of efficient factor for SiO_2/Ag core-shell nanoparticles shift to long wavelength side which directly leads to the shifting of negative permittivity tensors to other wavelength. The position of scattering peak depends on the radius of core and shell, so that we can achieve such materials for different working wavelength by adjusting the radius of core-shell nanoparticles. In addition, the permittivity of core material also influences the position of the scattering peak. By changing the core materials, such kind of HMs can be achieved from visible to near-infrared wavelength range.

4. Loss compensation

Due to the surface plasmon resonance, such kind of HMs suffers strong energy losses. As a result, loss compensation becomes very important. The energy loss could be compensated by incorporating gain materials into the metamaterial structures [28] and the experimental works have already been done in metal-dielectric fishnet structures [29]. In contrast to the difficult gain incorporation in other artificial metamaterials, it is very convenient to compensate the energy absorption by distributing active medium such as dye molecule into LCs [19].

Consider the compensation process of dye molecule as a two-level model. The system contains LC, silver nanoparticles and dye medium. The susceptibility of the dye medium is characterised by the form $\chi = \chi' + i\chi''$, where the real part χ' and imaginary part χ'' are described as follows [19]:

$$\chi' = \chi_{\max} \frac{2(\nu - \nu_0)/\Delta\nu}{1 + 4(\nu - \nu_0)^2/\Delta\nu^2}$$
$$\chi'' = \chi_{\max} \frac{1}{1 + 4(\nu - \nu_0)^2/\Delta\nu^2} \tag{10}$$

The parameter $\chi_{\max}$ is the maximum imaginary value and ν is the incident frequency. The centre frequency $\nu_0 = 6 \times 10^{14} Hz$ and the frequency linewidth $\Delta\nu = 6 \times 10^{12} Hz$.

The permittivity of the combined material changes from $\varepsilon_{\mathrm{LC}}$ to $\varepsilon_{\mathrm{host}} = \varepsilon_{\mathrm{LC}} + \chi$ in the effective permittivity calculations. The calculation parameters are same as in Section 3.1. The susceptibility of gain dye molecule depends on $\chi_{\max}$ when ν_0 $\Delta\nu$ are fixed. Figure 6 shows the real and imaginary parts of effective permittivity of the dye medium and nanoparticle

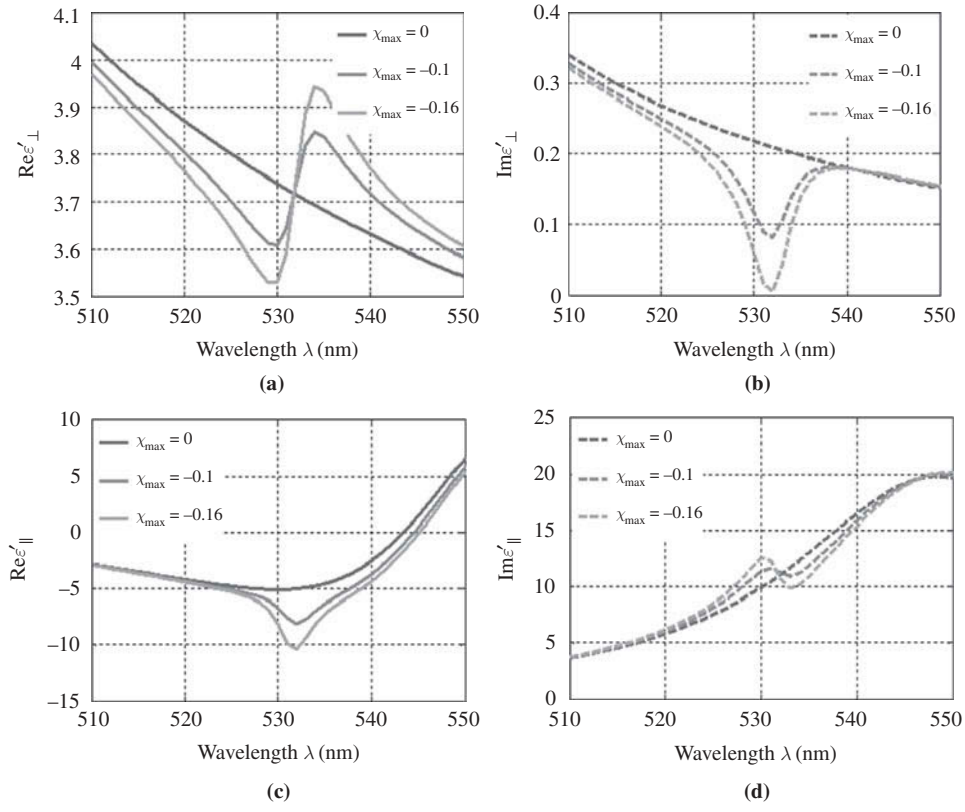

Figure 6. (colour online) (a) (c) Real and (b) (d) imaginary parts of the effective permittivities of silver nanoparticles dispersed dye-doped nematic liquid crystal.

dispersed LC. The χ_{max} of dye medium is 0, −0.1 and −0.16. We can see that from Figure 6 the gain medium not only changes the imaginary part but also the real part. At the resonance frequency, the imaginary part of $\varepsilon'_{\perp}$ is reduced as shown in Figure 6(b) and the real part of $\varepsilon'_{||}$ also becomes smaller as shown in Figure 6(c). Smaller $\mathrm{Im}(\varepsilon'_{\perp})$ means lower energy losses. The energy losses and the real part of effective permittivity both can be reduced by increasing the χ_{max}. The core-shell HM mentioned in Section 3.2 has the similar effects with dye medium.

5. Conclusions

In this work, a novel approach using self-aligned LC containing randomly dispersed nanoparticles is proposed for designing optical HMs. Due to the Mie scattering of spherical nanoparticle, permittivity tensors with opposite signs are achieved. By using core-shell nanoparticles, operating wavelength can be adjusted from visible to near-infrared. Gain medium can be introduced to reduce the energy losses. It also should be noted that the proposed material can be used to develop the flexible and tunable optical HMs because of the flexibility and easily controlled molecule direction of LCs.

Funding

This work is supported by the National Science Foundation of China [grant number 11174274], [grant number 11174279], [grant number 61205021], [grant number 11204299]; the Science Foundation of State Key Laboratory of Applied Optics.

References

[1] Wangberg R, Elser J, Narimanov EE, Podolskiy VA. Nonmagnetic nanocomposites for optical and infrared negative-refractive-index media. J Opt Soc Am B. 2006;23:498–505.
[2] Yao J, Liu Z, Liu Y, Wang Y, Sun C, Bartal G, Stacy AM, Zhang X. Optical negative refraction in bulk metamaterials of nanowires. Science. 2008;321:930.
[3] Liu H, Shivanand, Webb KJ. Subwavelength imaging with nonmagnetic anisotropic bilayers. Opt Lett. 2009; 34:2243–2245.
[4] Yao J, Tsai KT, Wang Y, Liu Z, Bartal G, Wang YL, Zhang X. Imaging visible light using anisotropic metamaterial slab lens. Opt Express. 2009;17:22380–22385.
[5] Ni X, Naik G, Kildishev A, Barnakov Y, Boltasseva A, Shalaev V. Effect of metallic and hyperbolic metamaterial surfaces on electric and magnetic dipole emission transitions. Appl Phys B. 2011;103:553–558.
[6] Poddubny AN, Belov PA, Ginzburg P, Zayats AV, Kivshar YS. Microscopic model of Purcell enhancement in hyperbolic metamaterials. Arxiv preprint arXiv:1205.3955. 2012.
[7] Naik GV, Liu J, Kildishev AV, Shalaev VM, Boltasseva A. Demonstration of Al: ZnO as a plasmonic component for near-infrared metamaterials. Proc Natl Acad Sci. 2012;109:8834–8838.
[8] Salandrino A, Engheta N. Far-field subdiffraction optical microscopy using metamaterial crystals: theory and simulations. Phys Rev B. 2006;74:075103.
[9] Jacob Z, Alekseyev LV, Optical Hyperlens NE. Far-field imaging beyond the diffraction limit. Opt Express. 2006;14:8247.
[10] Liu ZW, Lee H, Xiong Y, Sun C, Zhang X. Far-field optical hyperlens magnifying sub-diffraction-limited objects. Science. 2007;315:1686–1686
[11] Cortes C, Newman W, Molesky S, Jacob Z. Quantum nanophotonics using hyperbolic metamaterials. J Opt. 2012;14:063001.
[12] Noginov MA, Barnakov YA, Zhu G, Tumkur T, Li H, Narimanov EE. Bulk photonic metamaterial with hyperbolic dispersion. Appl Phys Lett. 2009;94:151105.
[13] Kanungo J, Schilling J. Experimental determination of the principal dielectric functions in silver nanowire metamaterials. Appl Phys Lett. 2010;97:021903.
[14] Hoffman AJ, Alekseyev L, Howard SS, Franz KJ, Wasserman D, Podolskiy VA, Narimanov EE, Sivco DL, Gmachl C. Negative refraction in semiconductor metamaterials. Nat Mater. 2007;6:946–950.
[15] Wheeler MS, Aitchison JS, Mojahedi M. Three-dimensional array of dielectric spheres with an isotropic negative permeability at infrared frequencies. Phys Rev B. 2005;72:193103.
[16] Khoo IC, Werner DH, Liang X, Diaz A, Weiner B. Nanosphere dispersed liquid crystals for tunable negative-zero-positive index of refraction in the optical and terahertz regimes. Opt Lett. 2006;31:2592–2594.
[17] Wheeler MS, Aitchison JS, Mojahedi M. Coated nonmagnetic spheres with a negative index of refraction at infrared frequencies. Phys Rev B. 2006;73:045105.
[18] Garcia-Etxarri A, Gomez-Medina R, Froufe-Perez LS, Lopez C, Chantada L, Scheffold F, Aizpurua J, Nieto-Vesperinas M, Saenz JJ. Strong magnetic response of submicron Silicon particles in the infrared. Opt Express. 2011;19:4815–4826.
[19] Khoo IC, Diaz A, Liou J, Stinger MV, Huang JB, Ma Y. Liquid crystals tunable optical metamaterials. IEEE J Sel Top Quantum Electron. 2010;16:410–417.
[20] Pawlik G, Jarema M, Walasik W, Mitus AC, Khoo IC. Field-induced inhomogeneous index distribution of a nano-dispersed nematic liquid crystal metamaterial near the Freedericksz transition: Monte Carlo studies. J Opt Soc Am B. 2010;27:567–576.
[21] Doyle WT. Optical properties of a suspension of metal spheres. Phys Rev B. 1989;39:9852–9858.
[22] Gauza S, Wen CH, Wu ST, Janarthanan N, Hsu CS. Super high birefringence isothiocyanato biphenyl-bistolane liquid crystals. Jpn J Appl Phys. 2004;43:7634–7638.
[23] Hovel H, Fritz S, Hilger A, Kreibig U, Vollmer M. Width of cluster plasmon resonances – bulk dielectric functions and chemical interface damping. Phys Rev B. 1993;48:18178–18188.
[24] Alvarez MM, Khoury JT, Schaaff TG, Shafigullin MN, Vezmar I, Whetten RL. Optical absorption spectra of nanocrystal gold molecules. J Phys Chem B. 1997;101:3706–3712.
[25] Palpant B, Prevel B, Lerme J, Cottancin E, Pellarin M, Treilleux M, Perez A, Vialle JL, Broyer M. Optical properties of gold clusters in the size range 2–4 nm. Phys Rev B. 1998;57:1963–1970.

[26] Rakic AD, Djurisic AB, Elazar JM, Majewski ML. Optical properties of metallic films for vertical-cavity optoelectronic devices. Appl Optics. 1998;37:5271–5283.
[27] Bohren CF, Huffman DR. Absorption and scattering of light by small particles. New York: Wiley-Interscience; 1983.
[28] Ramakrishna SA, Pendry JB. Removal of absorption and increase in resolution in a near-field lens via optical gain. Phys Rev B. 2003;67:201101.
[29] Xiao S, Drachev VP, Kildishev AV, Ni X, Chettiar UK, Yuan HK, Shalaev VM. Loss-free and active optical negative-index metamaterials. Nature. 2010;466:735–738.